A New Efficient Stiffness Evaluation Method to Improve Accuracy of Hexapods

Vinayak Jagannathrao Kalas, Alain Vissiere, Thierry Roux, Olivier Company, Sébastien Krut, François Pierrot

Proceedings of the ASME 2018 International Design Engineering Technical Conferences & Computers and Information in Engineering Conference
IDETC/CIE 2018
August 26- 29, 2018, Quebec City, Canada

DETC2018-85986

A NEW EFFICIENT STIFFNESS EVALUATION METHOD TO IMPROVE ACCURACY OF HEXAPODS

Vinayak J. Kalas*
Department of Robotics
LIRMM
34090 Montpellier, France
Email:vinayak.kalas@lirmm.fr

Alain Vissière
Department of Robotics
LIRMM
34090 Montpellier, France
Email: alain.vissiere@lirmm.fr

Thierry Roux
Symétrie
10 Allée Charles Babbage, 30035 Nîmes
France
Email: thierry.roux@symetrie.fr

Olivier Company
Department of Robotics
LIRMM
34090 Montpellier, France
Email: olivier.company@lirmm.fr

Sébastien Krut
Department of Robotics
LIRMM
34090 Montpellier, France
Email: sebastien.krut@lirmm.fr

François Pierrot
Department of Robotics
LIRMM
34090 Montpellier, France
Email: francois.pierrot@lirmm.fr

ABSTRACT

Structural compliance of hexapod positioners limits their positioning accuracy. Taking a step towards solving this problem, this paper proposes a new efficient method to evaluate the stiffness of hexapods in order to predict and correct their positioning error due to compliance. The proposed method can be used to predict the six degree of freedom deflection of the platform under load. This method uses a simple lumped stiffness parameter model whose parameters can be estimated using the identification technique presented in this paper. An experimental study with micrometer level measurements performed on a hexapod based micro-positioning system is used to assess the efficiency of the presented method.

INTRODUCTION

Hexapods, also called Gough-Stewart platforms, are increasingly used for applications demanding high accuracy six degree of freedom (DOF) positioning. Some general areas of applications include mirror positioning in telescopes [1], positioning components in synchrotrons [2] and research applications demanding high accuracy positioning [3]. One of the biggest advantages of hexapods is their high inherent stiffness [4]. Hence, in most applications, hexapod compliance doesn't considerably degrade the accuracy of positioning. However, as accuracy requirements become more stringent, quantifying the hexapod's compliance error becomes crucial in order to correct it. This work forms a part of a larger project, Posilab [5], that is focused on improving the performance of the current state of the art hexapod positioners. The work presented in this paper focusses on solving the problem of platform deflection due to hexapod compliance. The developed solution needed to be applicable to existing hexapods. Hence, redesigning the hexapod was not a feasible option. It was, therefore, necessary for the solution developed in this work to be applicable in a position compensation framework. This can be achieved by using a model-based approach to estimate hexapod compliance. This approach would encompass choosing a suitable stiffness parameter model followed by identification of these parameters using appropriate measurements [6].

Stiffness modelling of parallel robots has acquired vast attention in research leading to development of very simple stiff-

*Address all correspondence to this author.

ness matrix [7] to an advanced one [8]. To be included in a position compensation framework, it is crucial to accurately predict platform deflection. This needs accurate prediction of the parameters of the stiffness model. This problem has been mainly approached in research in the following directions: (a) analytical estimation of stiffness model parameters, this option has been widely addressed in literature [9–16], and (b) stiffness parameter identification using measurements, which is a relatively new approach [6,17–23]. In many cases, analytically estimated stiffness parameters do not lead to accurate deflection predictions of end-effector/platform. Also, the latter option has the advantage of being analytically simple and less time-consuming as it doesn't involve cumbersome calculations. These reasons make option (b) very attractive for implementation in an industrial framework and hence, this method is suitable for our application.

The accuracy of robot model parameters identified using measurements is largely dependent on the robot poses used, external forces used and the number of measurements performed. Therefore, the identification procedure needs to be optimized to obtain best set of parameters. The concept of parameter observability addresses this issue. This has been discussed in detail in the 'Stiffness identification method' section.

Stiffness identification technique has been applied very well to serial robots [6], [18–21], [24]. One of the most advanced stiffness identification methods for serial robots has been presented by Dumas et al. [21]. In this work, the observability of parameters was defined based on an advanced stiffness model. Klimchik et al. [18] also presented a robust stiffness identification method that used a simple stiffness model. They optimized their identification to improve accuracy at the intended operational configuration of a 6-R serial robot.

Stiffness identification has not been used much for evaluating stiffness of parallel robots yet. Carbone et al. [22] evaluated the stiffness of a 3-DOF parallel manipulator CaPaMan by measuring displacements of the platform under load. However, this method was not optimized to obtain the best set of parameters. Bonnemains et al. [23] evaluated the stiffness of a 3-DOF tricept parallel robot. This work, too, did not address parameter observability satisfactorily. No work so far, to the best of authors' knowledge, has demonstrated a complete and robust stiffness identification method for parallel robots. Also, no stiffness identification method has been presented for a hexapod system.

The method to be developed for the application concerned to this paper had to be directly applied in the industry. It was, therefore, very important for the stiffness evaluation method to be simple while being accurate enough. It is also desirable to have a less time consuming method in an industrial framework. These factors facilitate the use of a simple stiffness matrix as presented in [7].

This paper presents a method to identify the components of the Cartesian stiffness matrix of hexapods by means of measurements. This method only requires a small number of tests to be carried out. The method uses a simple lumped stiffness parameter model that uses only one spring per leg to model the overall stiffness. An observability index is then used to find the best set of poses and forces for parameter identification. The choice of this index is also discussed. Finally, the efficiency of the proposed method is validated by means of experiments: the predicted 6-DOF deflection of platform under load is compared to the measured values. The experimental study is performed on a micro-positioning system developed by Symétrie [25], a manufacturer of high-precision hexapod positioners. The analysis in this paper is demonstrated using a spherical-prismatic-spherical (SPS) hexapod positioner. However, this method is also valid for other sorts of hexapods: universal-prismatic-universal (UPU), UPS and SPU.

This paper is organised as follows: Firstly, the kinematics and stiffness model of a general SPS hexapod is shown. The method for stiffness identification is then presented. This is followed by a brief description of the measurement technique used to measure the 6-DOF pose parameters and displacement of the hexapod. The implementation and experimental validation of the stiffness identification method is then presented. The results and the intended future work are then discussed followed by conclusions on the work presented in this paper.

KINEMATICS AND STIFFNESS MODEL

Fig. 1 shows the schematic of a general SPS hexapod. Each leg consists of a SPS chain that connects to the base at points A_i and to the platform at points B_i. Two frames of references are defined for the sake of analysis, the fixed frame of reference R_f and the mobile frame of reference R_m(fixed to the platform). R_f and R_m align exactly with each other when the platform is in nominal position. The connection points A_i and B_i lie on circles with centers O_b and O_m, respectively.

The platform pose, given by X, can be written as,

$$X = [a, b, c, \alpha, \beta, \gamma]^T \tag{1}$$

The first three elements of X represent the translation along X, Y and Z axes of the mobile frame of reference, R_m. α, β and γ are the angular rotations of the platform around X, Y and Z axes of the same frame. The angles are defined as per X-Y-Z extrinsic Euler convention. q contains the lengths of six prismatic links.

$$q = [q_1, q_2, q_3, q_4, q_5, q_6]^T \tag{2}$$

A simple lumped stiffness model (as shown in Fig. 2) is used to model the static stiffness characteristics of this mechanism. One spring is used to model the stiffness of each leg ($k_{\text{i=1 to 6}}$). This model assumes that the actuators are the main contributors of

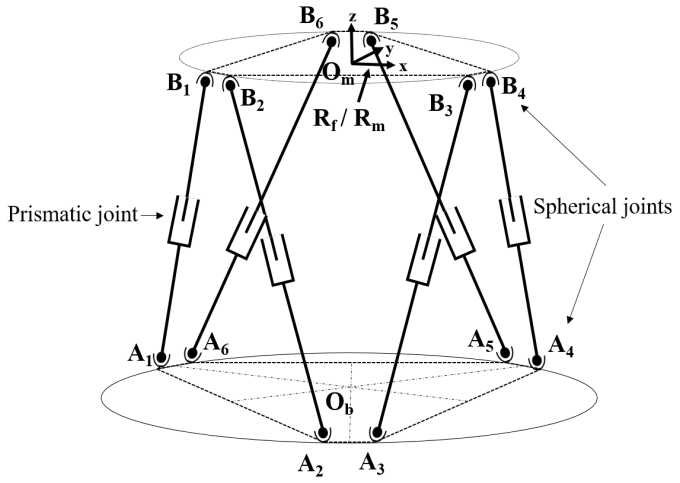

FIGURE 1. Schematic of a SPS hexapod

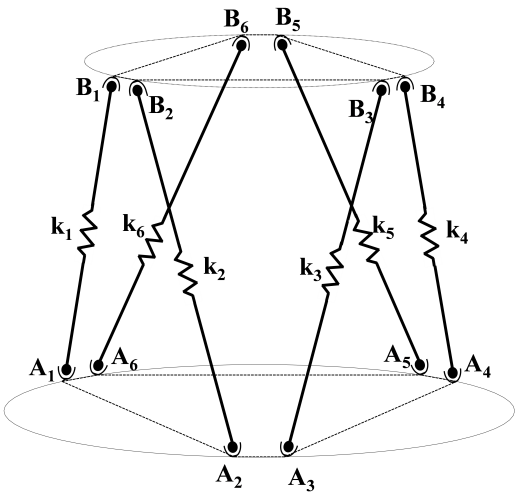

FIGURE 2. Lumped stiffness model of the SPS hexapod

compliance and that the rest of the structure is rigid. The joints are assumed to be frictionless. Also, the legs of the hexapod are assumed massless and considered to be subjected to axial loads only.

The relationship between the platform velocity vector and the joint velocity vector is given by,

$$\dot{q} = J^{-1}V \tag{3}$$

Here, V contains the components of velocity of the platform. J is the jacobian matrix of the hexapod which is evaluated as per method outlined in [26]. Now, the relationship between differential leg lengths and the differential platform pose (Δq and ΔX) can be written as,

$$\Delta q = \widetilde{J}^{-1}\Delta X \tag{4}$$

Here, $\widetilde{J}^{-1}$ is given by,

$$\widetilde{J}^{-1} = J^{-1}\begin{bmatrix} I & 0 \\ 0 & M \end{bmatrix} \tag{5}$$

In equation (5), I is a 3×3 identity matrix and matrix M is given by,

$$M = R \times \begin{bmatrix} 1 & 0 & -s_\beta \\ 0 & c_\alpha & c_\beta.s_\alpha \\ 0 & -s_\alpha & c_\beta.c_\alpha \end{bmatrix} \tag{6}$$

Here, $c_\bullet = cos(\bullet)$ and $s_\bullet = sin(\bullet)$. R in equation (6) is the rotation matrix given by,

$$R = \begin{bmatrix} c_\gamma.c_\beta & -s_\gamma.c_\alpha + c_\gamma.s_\beta.s_\alpha & s_\gamma.s_\alpha + c_\gamma.s_\beta.c_\alpha \\ s_\gamma.c_\beta & c_\gamma.c_\alpha + s_\gamma.s_\beta.s_\alpha & -c_\gamma.s_\alpha + s_\gamma.s_\beta.c_\alpha \\ -s_\beta & c_\beta.s_\alpha & c_\beta.c_\alpha \end{bmatrix} \tag{7}$$

The operation shown in equation (5) is necessary because $\widetilde{J}$ relates the derivatives of components of X to the derivatives of components of q. Hence, J^{-1} from equation (3) needs to be altered to take into account the relationship between angular velocities and angle derivatives as per X-Y-Z extrinsic Euler convention as shown in [27]. Now, the Cartesian stiffness matrix K_C of this parallel system can be expressed as:

$$K_C = J^{-\mathrm{T}} K \widetilde{J}^{-1} \tag{8}$$

Matrix K is diagonal matrix with leg stiffnesses forming its diagonal elements as shown in equation (9).

$$K = \begin{bmatrix} k_1 & 0 & 0 & 0 & 0 & 0 \\ 0 & k_2 & 0 & 0 & 0 & 0 \\ 0 & 0 & k_3 & 0 & 0 & 0 \\ 0 & 0 & 0 & k_4 & 0 & 0 \\ 0 & 0 & 0 & 0 & k_5 & 0 \\ 0 & 0 & 0 & 0 & 0 & k_6 \end{bmatrix} \tag{9}$$

The matrix K_C relates the 6×1 wrench vector ΔF applied at the platform and the 6×1 platform displacement vector ΔX as,

$$\Delta F = K_C \Delta X \tag{10}$$

Equation (10) can be reorganized to get the following equation:

$$Ax = \Delta X \tag{11}$$

Here, x is a 6×1 vector that contains joint compliances $1/k_i$.

$$x = [1/k_1, 1/k_2, 1/k_3, 1/k_4, 1/k_5, 1/k_6]^T \tag{12}$$

The 6×6 matrix A is a function of ΔF, $\widetilde{J}$ and J. The elements of A are given by,

$$A_{\mathrm{ij}} = \widetilde{J}_{\mathrm{ij}} \left(\sum_{k=1}^{6} J_{\mathrm{kj}} \Delta F_k \right) \tag{13}$$

Here, i, j and k are the subscripts for the row and column of respective matrices. $\Delta F_{\mathrm{k=1\ to\ 6}}$ refer to the components of wrench applied to the platform.

STIFFNESS IDENTIFICATION METHOD

Method description

When we substitute the values of estimated lumped stiffnesses ($k_{\mathrm{i=1\ to\ 6}}$), wrench ΔF, hexapod jacobian J and $\widetilde{J}$ in equation (11), we get the expected platform deflection ΔX. The same equation can be used to identify lumped stiffness values when we know everything in equation (11) except x. This implies loading the platform, measuring the platform deflection and solving equation (11). If we increase the number of poses to be measured, we get a $6n \times 1$ x vector and a $6n \times 6$ A matrix, where n is the number of poses.

Fig. 3 shows the procedure for stiffness identification. It consists of the following steps:

1. Define experimental constraints that restrict the identification process. For example: workspace limits, loading limitations, etc.
2. Choose the number of poses and the number of measurements per pose. More number of measurements per pose help to reduce the uncertainty of identified parameters at a given pose due to measurement errors.
3. Identify the best set of poses (considering workspace constraints) and corresponding external forces (considering loading constraints) to identify the stiffness parameters. The next sub-section elaborates on the need and method for choosing the optimal set of poses and forces.
4. Load the platform suitably at identified best poses and measure the 6-DOF platform deflection.
5. Solve equation (11) to obtain the vector x. This can be accomplished by minimizing the Euclidean norm of $(Ax - \Delta X)$. The MATLAB function *lsqminnorm* can be used for this purpose.

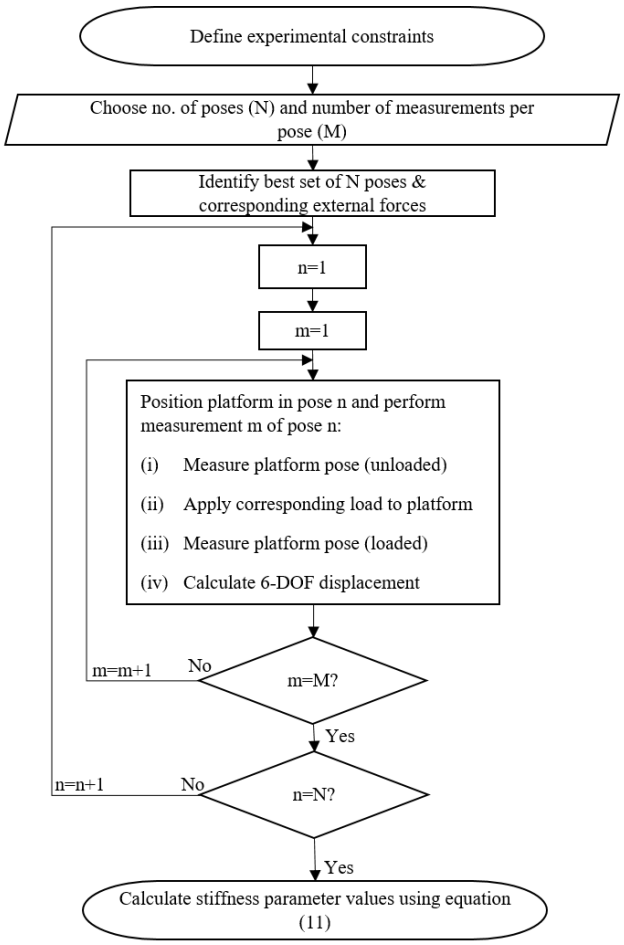

FIGURE 3. Procedure for stiffness identification

Algorithm to identify optimal set of poses and forces

The idea behind having measurements at more number of poses is the same as that for robot geometric calibration. In geometric calibration, measurements of large number of poses spread across the robot's workspace are used. These measurements are then used to get the best geometric parameter set that minimizes the error between commanded and attained robot pose throughout the workspace. Large number of poses are needed for this to reduce the influence of measurement errors. However,

practicality concerns demand reduction of these measurements. It has been shown that choosing the right set of measurement poses improves identification accuracy [28].

In our application, matrix A decides the quality of identification of parameters. This is because it relates the measurements done to the identified parameters. Since A is a function of X and ΔF, the best parameters can be identified by judicious choice of robot poses X and platform forces ΔF. Hence, the parameters need to be optimized for all reachable poses and allowable forces.

Parameter identification observability is a well-researched topic in robot calibration literature. However, stiffness parameter identification observability is a relatively new area of research. Klimchik et al. [18] have presented a method to optimize the pose set for stiffness parameter identification to increase the accuracy of displacement prediction at just one particular pose. This is not suitable for us since we seek to increase the accuracy of displacement prediction throughout the workspace of the hexapod.

Many observability indices can be found in the calibration literature: O_1 [28], O_2 [29], O_3 [30], O_4 [31] and O_5 [32]. The reliability and performance of these observability indices have been studied very well too [32–37]. There is no absolute consensus on the best observability index and also their performances have been noted to depend on the type of robot being calibrated [36]. Joubair et al. [34] have also shown that all these observability indices yield good result when the measurement noise is low.

The observability indices also depend on the properties of robot models. Matrix scaling needs to be employed when parameters for different variables with different units need to be identified in calibration. Also, different scaling approaches produce different results. Only O_1 is suitable for optimization of parameter estimation with unscaled robot models. The mathematical proof for this can be found in [32]. If this stiffness identification technique is to be later included in a complete calibration technique that also includes geometric parameters, the issue of matrix scaling can be more complex. Therefore, to avoid complications related to matrix scaling, it is advantageous to select O_1 as the observability index.

For stiffness parameter identification using equation (11), O_1 is obtained by singular value decomposition of matrix A. It can be calculated as shown in [28],

$$O_1 = \frac{(\sigma_1\sigma_2\sigma_3....\sigma_p)^{1/p}}{\sqrt{N}} \tag{14}$$

Here, p is the number of parameters to be identified which in our case is 6 and N is the number of poses. $\sigma_{1\text{ to p}}$ are the singular values of matrix A. The best set of poses and corresponding external forces maximize the index O_1. An optimization routine then needs to be used to find the best set of poses and external forces that maximize O_1.

MEASUREMENT TECHNIQUE

This section elaborates on the measurement technique used to measure the hexapod pose parameters in the experiments presented in this paper. The measurement setup is as shown in Fig. 4. The measurement system consists of a LK-METRIS coordinate measuring machine (CMM) with RENISHAW SP25M scanning probe. Precision balls are glued to the hexapod for measurement of poses using the CMM. The procedure can be divided into two steps: (i) identifying the coordinate frame fixed to the mobile platform, and (ii) measurement of poses using precision balls. The interest here is to measure the 6-DOF parameters, X, of the platform pose by measuring the positions of precision balls in space.

The identification of reference frame fixed to the mobile platform is done in the manner similar to the one described in [38]. The reference holes on the hexapod are used for this purpose. These reference holes are machined into the platform of the hexapod in the production phase. This is followed by measuring the positions of three precision balls with reference to the mobile frame. These three balls' positions can then be used as three points in space to identify the mobile frame.

The measurement technique can be demonstrated using Fig. 5. Let *Pose* 1 be the pose in which the precision balls are identified in the mobile frame. Let P_{A1}, P_{B1} and P_{C1} be the positions of the three precision balls associated with this pose and expressed in the mobile frame of reference. The pose vector X_1 associated with this pose is $[0,0,0,0,0,0]^T$. Let's call this measurement $M1$. Now, when the platform moves to *Pose* 2, we carry out measurement $M2$ of the precision balls' positions: P_{A2}, P_{B2} and P_{C2}. The precision balls' positions of measurement $M2$ are also expressed in mobile frame. A least square fitting algorithm is then used to superimpose the relative positions of the balls measured in $M1$ on to the ball positions measured in $M2$. The mobile frame associated with *Pose* 2 can then be easily identified since the pose of mobile frame relative to precision balls' positions (P_{A1}, P_{B1} and P_{C1}) of *Pose* 1 is known. We now obtain *Pose* 2 (X_2) with respect to *Pose* 1. Subsequent poses can then be measured with respect to *Pose* 1. All this is done automatically using dedicated software tools developed by Symétrie. The 6-DOF deflection between the poses can be obtained by subtracting X_1 from X_2.

METHOD IMPLEMENTATION AND EXPERIMENTAL VALIDATION

This section elaborates on how the stiffness identification method was used to evaluate stiffness of a hexapod positioner from Symétrie. The product details cannot be disclosed due to confidentiality. The test setup is as shown in Fig. 6.

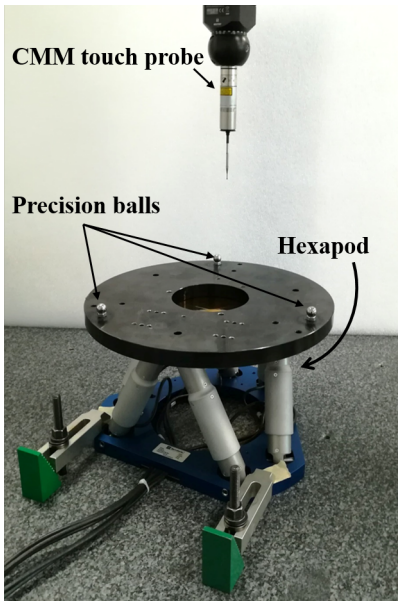

FIGURE 4. Measurement setup

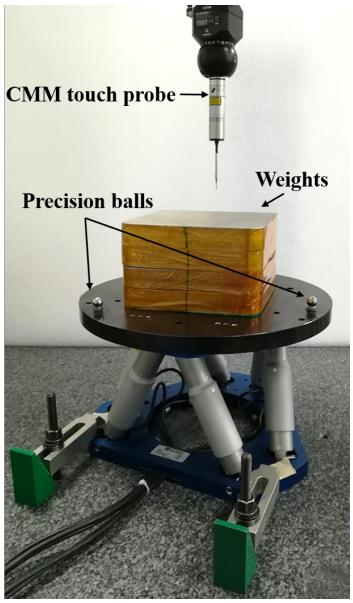

FIGURE 6. Experimental setup

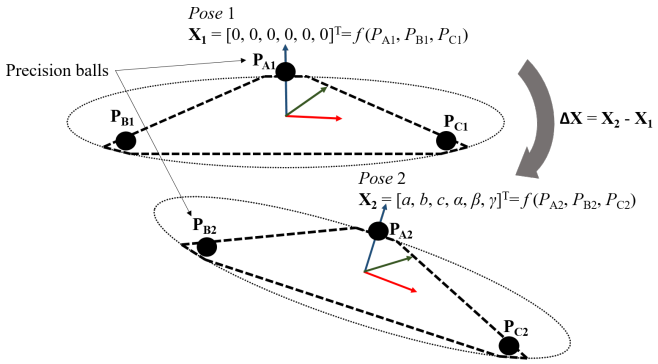

FIGURE 5. Pose measurement using precision balls

The experimental constraints included: (i) the allowable workspace of the robot, and (ii) the loading constraint. Concerning the workspace constraints for identification, the platform could not be rotated around its X and Y axes in addition to allowable workspace of the hexapod. This constraint was incorporated to make sure that the mounted mass doesn't slide off the platform. The loading constraint in this case was that the platform could only be loaded by placing mass on it. The load was, therefore, along the Z axis of the platform.

Now, the number of poses and number of measurements per pose had to be chosen. For any system of equations, the number of equations should at least be equal to the number of unknowns. In this case, we have 6 unknowns and each pose measurement gives us six equations (6-DOF measurement). Hence, just one measurement is analytically enough to identify all parameters. For efficiency, it is also desirable to keep the number of poses for identification less. Hence, compromising between efficiency and accuracy, 3 poses and 3 measurements per pose were chosen. This choice would lead to a total of 9 measurements for identification. Given the nature of measurements in our case, this result in 54 equations for 6 unknowns.

These choices and constraints lead to 13 design variables for the optimization: twelve pose variables and one force variable. Concerning the load variable, ΔF_3, further analysis revealed that the index O_1 increased with increased magnitude of ΔF_3 for any random set of poses (Fig. 7). It was also observed that the hexapod has linear stiffness characteristics. Fig. 8 shows the results of an experiment that shows the hexapod's linear stiffness behavior. In this case, the hexapod platform was loaded only along its Z-axis at pose $[0,0,0,0,0,0]^T$. Due to these reasons, a choice was made to use just one load vector of maximum possible magnitude to induce maximum platform deflection. This was 34.5 kg in the given case. For displacement calculation, the reference condition was a pre-load of 12.2 kg. This was necessary to suppress the play in actuators. Hence, the effective load for which the platform deflection was measured was 22.3 kg along the Z-axis of the platform. It must be noted that in cases where stiffness is considerably dependent on applied force, more loading conditions will have to be considered for this optimization.

Since the force variable was already chosen, the number of design variables reduced to 12. MATLAB's *fmincon* function was then used to find the best set of 3 configurations that gave the highest O_1. These results are very sensitive to the starting point supplied to the optimization algorithm. To tackle this, par-

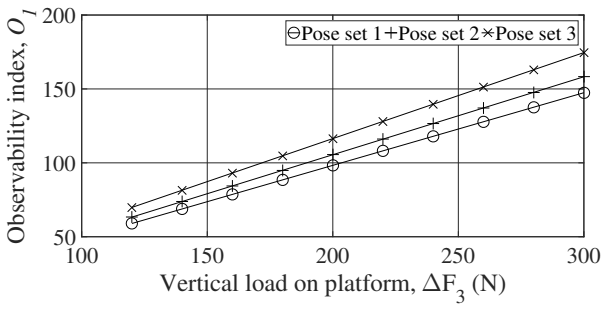

FIGURE 7. Trend of O_1 with respect to ΔF_3

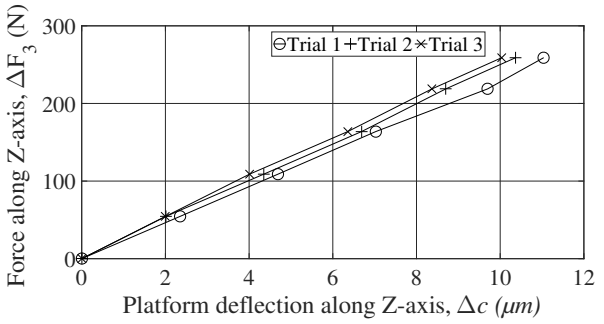

FIGURE 8. Plot showing linear stiffness behavior of hexapod under study

allel computing was used along with large number of starting points to find the best solution. The best pose set for identification generated by this optimization is shown in table 1. The hexapod was loaded in these poses and the platform deflections were measured. Equation (11) was then solved to get the stiffness parameters which are tabulated in table 2.

TABLE 1. Best pose set for stiffness identification

	$a(mm)$	$b(mm)$	$c(mm)$	$\alpha(deg)$	$\beta(deg)$	$\gamma(deg)$
*Pose*1	2.616	0.832	-0.666	0	0	15.756
*Pose*2	10.017	-3.434	-0.764	0	0	-11.007
*Pose*3	-7.784	-3.210	1.760	0	0	-11.266

The efficiency of this stiffness identification method was then validated using platform deflection measurements done at different poses along the X and Y axes of the hexapod. The detailed description of poses is tabulated in table 3. The load used was same as that for stiffness identification. Figures 9 and 10 show the comparison between the predicted and measured 6-DOF deflections of the platform at different poses along the X and Y axes of the hexapod, respectively. Table 4 shows the RMS values of error in prediction of the 6-DOF deflections.

TABLE 2. Identified stiffness parameters

Stiffness parameter value $(N/\mu m)$					
k_1	k_2	k_3	k_4	k_5	k_6
4.1981	3.7898	2.7503	4.3200	3.6716	3.7288

TABLE 3. Pose set for experimental validation

Pose along	Pose parameters					
	$a(mm)$	$b(mm)$	$c(mm)$	$\alpha(deg)$	$\beta(deg)$	$\gamma(deg)$
X-axis	-30	0	0	0	0	0
	-15					
	0					
	15					
	30					
Y-axis	0	-30	0	0	0	0
		-15				
		0				
		15				
		30				

TABLE 4. Error in deflection prediction (RMS values)

$\varepsilon_{\Delta a}$	2.7 μm
$\varepsilon_{\Delta b}$	3.1 μm
$\varepsilon_{\Delta c}$	2.2 μm
$\varepsilon_{\Delta \alpha}$	6.4 μrad
$\varepsilon_{\Delta \beta}$	8.3 μrad
$\varepsilon_{\Delta \gamma}$	8.8 μrad

DISCUSSION AND FUTURE WORK

Validation results show that the predicted and measured deflections of the platform are very close. As seen from table 4, the RMS values of prediction error is under 3.1 μm for translational deflections and 8.8 μrad for rotational deflections. This method

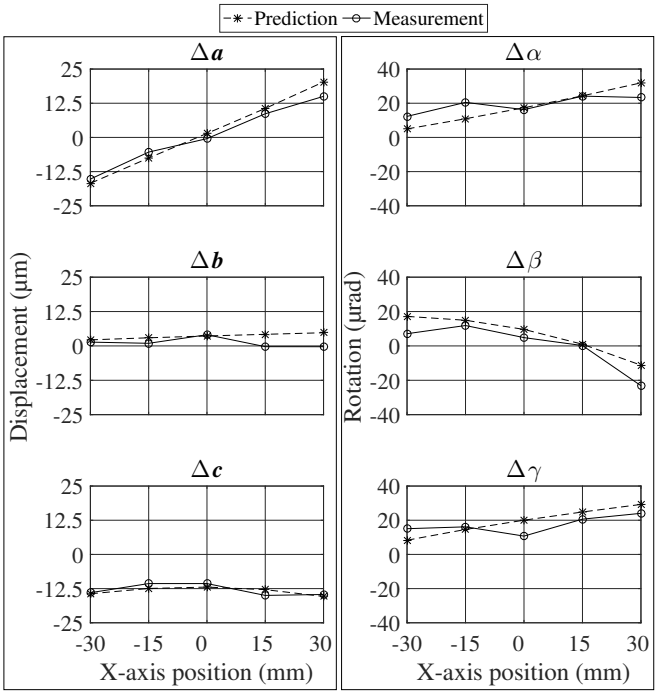

FIGURE 9. Plot of predicted and measured 6-DOF deflection of hexapod under load at poses along X-axis

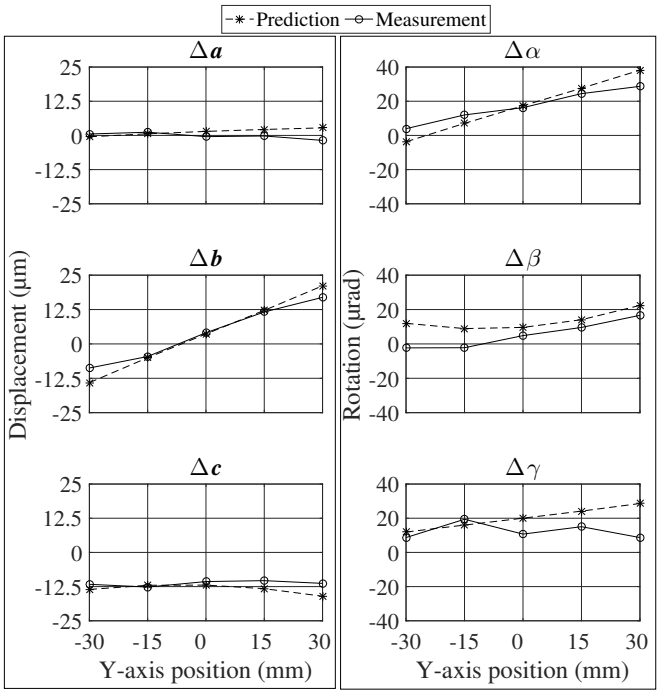

FIGURE 10. Plot of predicted and measured 6-DOF deflection of hexapod under load at poses along Y-axis

will also reduce the positioning inaccuracy due to compliance of the hexapod to the same level. This is due to the fact that the model prediction accuracy is the only source of error in position compensation technique. This implies that the positioning error due to compliance deflection will reduce, for example, along Z-axis translational coordinate of the hexapod from 13.5 μm (RMS value of measured Δc) to 2.2 μm.

The small difference that exists between the prediction and the measured values could be attributed to the following:

1. Uncertainty of measurement of the measurement system: All measurements have an uncertainty bound and this limits both stiffness parameter identification and the experimental validation.
2. Geometric parameter error: The geometric parameters of the hexapod used for analysis was not calibrated. This is a source of error in parameter identification and experimental validation. This is because of the use of an erroneous geometric model to identify stiffness parameters from the measurements and for predicting the displacements.
3. Incomplete stiffness model: The simple stiffness model used cannot capture the complete compliance behavior of the hexapod. Consequently, there will be some residual error due to unmodelled compliance.

For future works, the method presented in this paper will, firstly, be validated for other loading conditions such as loading along X and Y axes of the platform. It will also be validated for other hexapod mounting conditions in which some or all legs are subjected to tensile loading. These studies are of interest to validate the efficacy of the presented method to improve accuracy of positioning in applications such as the one shown in [39]. This method will then be extended to include geometric and thermal parameter models to further improve the positioning accuracy of the hexapod.

CONCLUSION

This paper proposed a new efficient method to experimentally evaluate the stiffness of hexapods. This can be used to accurately predict and correct its positioning error due to structural compliance. The method employed a simple lumped stiffness parameter model which uses one spring per leg to mimic its compliance behavior. A stiffness identification procedure was outlined to estimate the parameters of the proposed stiffness model. This method required small number of measurements. An optimization based on an observability index was used to generate the best set of poses and external forces for stiffness parameter identification. The efficiency of the presented method was evaluated using an experimental study performed on a hexapod based micro-positioner. This was done by comparing the predicted 6-DOF deflections of the platform with the measured deflections. Results showed that the chosen model with identified parame-

ters could predict and consequently allow to correct the platform deflections of the tested hexapod very well. The RMS values of prediction error in the validation experiments is under 3.1 μm for translational deflections and 8.8 μrad for rotational deflections. The method is shown to reduce the RMS of positioning error due to compliance deflection, for example, along the Z-axis translational coordinate of the hexapod from 13.5 μm to 2.2 μm.

ACKNOWLEDGMENT

This work has been supported by Agence nationale de la recherche (ANR), France (Projet ANR-15-LCV3-0005). The authors hereby express their gratitude for the support. The authors would like to thank Marielle Baud from Symétrie for the help provided in using CMM. The authors would also like to acknowledge the valuable inputs from Olivier Lapierre, Gilles Diolez, Pierre Noire and Tristan Caritey of Symétrie.

REFERENCES

[1] Symétrie. Telescope mirror adjustment. `http://www.symetrie.fr/en/applications-2/telescope-mirror-adjustment/`. [Accessed: 2018-03-08].

[2] Symétrie. Hexapods for synchrotrons. `http://www.symetrie.fr/en/applications-2/synchrotrons/`, [Accessed: 2018-03-08].

[3] Symétrie. High payload adjustment with high accuracy. `goo.gl/4eJXqp`. [Accessed: 2018-03-08].

[4] Merlet, J.-P., 2006. *Parallel robots*, Vol. 128. Springer Science & Business Media.

[5] LIRMM-Symétrie. Posilab. `http://www.lirmm.fr/posilab/`.

[6] Dumas, C., Caro, S., Chrif, M., Garnier, S., and Furet, B., 2010. "A methodology for joint stiffness identification of serial robots". In 2010 IEEE/RSJ International Conference on Intelligent Robots and Systems, pp. 464–469.

[7] Lee, K. M., and Johnson, R., 1989. "Static characteristics of an in-parallel actuated manipulator for clamping and bracing applications". In Proceedings, 1989 International Conference on Robotics and Automation, pp. 1408–1413 vol.3.

[8] Klimchik, A., Chablat, D., and Pashkevich, A., 2014. "Stiffness modeling for perfect and non-perfect parallel manipulators under internal and external loadings". *Mechanism and Machine Theory,* ***79***, pp. 1 – 28.

[9] Corradini, C., Fauroux, J.-C., Krut, S., et al., 2003. "Evaluation of a 4-degree of freedom parallel manipulator stiffness". In Proceedings of the 11th World Congress in Mechanisms and Machine Science, Tianjin (China).

[10] Majou, F., Gosselin, C., Wenger, P., and Chablat, D., 2007. "Parametric stiffness analysis of the orthoglide". *Mechanism and Machine Theory,* ***42***(3), pp. 296 – 311.

[11] Clinton, C. M., Zhang, G., and Wavering, A. J., 1997. Stiffness modeling of a stewart platform based milling machine. Tech. rep.

[12] Li, Y.-W., Wang, J.-S., and Wang, L.-P., 2002. "Stiffness analysis of a stewart platform-based parallel kinematic machine". In Proceedings 2002 IEEE International Conference on Robotics and Automation (Cat. No.02CH37292), Vol. 4, pp. 3672–3677 vol.4.

[13] Deblaise, D., Hernot, X., and Maurine, P., 2006. "A systematic analytical method for pkm stiffness matrix calculation". In Proceedings 2006 IEEE International Conference on Robotics and Automation, 2006. ICRA 2006., pp. 4213–4219.

[14] Chen, J., and Lan, F., 2008. "Instantaneous stiffness analysis and simulation for hexapod machines". *Simulation Modelling Practice and Theory,* ***16***(4), pp. 419 – 428.

[15] Rebeck, E., and Zhang, G., 1999. "A method for evaluating the stiffness of a hexapod machine tool support structure". *International Journal of Flexible Automation and Integrated Manufacturing,* ***7***(3/4), pp. 149–166.

[16] Klimchik, A., Pashkevich, A., and Chablat, D., 2013. "CAD-based approach for identification of elasto-static parameters of robotic manipulators". *Finite Elements in Analysis and Design,* ***75***, pp. 19 – 30.

[17] Carbone, G., and Ceccarelli, M., 2006. "A procedure for experimental evaluation of cartesian stiffness matrix of multibody robotic systems". In 15th CISM-IFToMM Symposium on Robot Design, Dynamics and Control, Romansy.

[18] Klimchik, A., Pashkevich, A., Wu, Y., Caro, S., and Furet, B., 2012. "Design of calibration experiments for identification of manipulator elastostatic parameters". *Journal of Mechanics Engineering and Automation,* ***2***, pp. 531–542.

[19] Alici, G., and Shirinzadeh, B., 2005. "Enhanced stiffness modeling, identification and characterization for robot manipulators". *IEEE Transactions on Robotics,* ***21***(4), Aug, pp. 554–564.

[20] Klimchik, A., Furet, B., Caro, S., and Pashkevich, A., 2015. "Identification of the manipulator stiffness model parameters in industrial environment". *Mechanism and Machine Theory,* ***90***, pp. 1 – 22.

[21] Dumas, C., Caro, S., Cherif, M., Garnier, S., and Furet, B., 2012. "Joint stiffness identification of industrial serial robots". *Robotica,* ***30***(4), p. 649659.

[22] Ceccarelli, M., and Carbone, G., 2005. "Numerical and experimental analysis of the stiffness performances of parallel manipulators". In Second international colloquium collaborative research centre, Vol. 562, pp. 21–35.

[23] Bonnemains, T., Chanal, H., Bouzgarrou, B.-C., and Ray, P., 2009. "Stiffness computation and identification of parallel kinematic machine tools". *Journal of Manufacturing*

Science and Engineering, ***131***(4), p. 041013.

[24] Abele, E., Weigold, M., and Rothenbcher, S., 2007. "Modeling and identification of an industrial robot for machining applications". *CIRP Annals,* ***56***(1), pp. 387 – 390.

[25] Symétrie. Experts in metrology and positioning. `http://www.symetrie.fr/en/company/`. [Accessed: 2018-03-08].

[26] Dombre, E., and Khalil, W., 2013. *Robot manipulators: modeling, performance analysis and control*. John Wiley & Sons.

[27] Ardakani, H. A., and Bridges, T., 2010. "Review of the 3-2-1 euler angles: a yaw-pitch-roll sequence". *Department of Mathematics, University of Surrey, Guildford GU2 7XH UK, Tech. Rep*.

[28] Borm, J. H., and Menq, C. H., 1989. "Experimental study of observability of parameter errors in robot calibration". In Proceedings, 1989 International Conference on Robotics and Automation, pp. 587–592 vol.1.

[29] Driels, M. R., and Pathre, U. S., 1990. "Significance of observation strategy on the design of robot calibration experiments". *Journal of Robotic Systems,* ***7***(2), pp. 197–223.

[30] Nahvi, A., Hollerbach, J. M., and Hayward, V., 1994. "Calibration of a parallel robot using multiple kinematic closed loops". In Proceedings of the 1994 IEEE International Conference on Robotics and Automation, pp. 407–412 vol.1.

[31] Nahvi, A., and Hollerbach, J. M., 1996. "The noise amplification index for optimal pose selection in robot calibration". In Proceedings of IEEE International Conference on Robotics and Automation, Vol. 1, pp. 647–654 vol.1.

[32] Sun, Y., and Hollerbach, J. M., 2008. "Observability index selection for robot calibration". In 2008 IEEE International Conference on Robotics and Automation, pp. 831–836.

[33] Horne, A., and Notash, L., 2009. "Comparison of pose selection criteria for kinematic calibration through simulation". In Computational Kinematics-Proceedings of the 5th International Workshop on Computational Kinematics, Springer, pp. 291–298.

[34] Joubair, A., and Bonev, I. A., 2013. "Comparison of the efficiency of five observability indices for robot calibration". *Mechanism and Machine Theory,* ***70***, pp. 254–265.

[35] Zhou, J., Kang, H.-J., and Ro, Y.-S., 2010. "Comparison of the observability indices for robot calibration considering joint stiffness parameters". In Advanced Intelligent Computing Theories and Applications, Springer, pp. 372–380.

[36] Joubair, A., Tahan, A. S., and Bonev, I. A., 2016. "Performances of observability indices for industrial robot calibration". In 2016 IEEE/RSJ International Conference on Intelligent Robots and Systems (IROS), pp. 2477–2484.

[37] Joubair, A., Nubiola, A., and Bonev, I., 2013. "Calibration efficiency analysis based on five observability indices and two calibration models for a six-axis industrial robot". *SAE International Journal of Aerospace,* ***6***(2013-01-2117), pp. 161–168.

[38] Zhang, G., Du, J., and To, S., 2016. "Calibration of a small size hexapod machine tool using coordinate measuring machine". *Proceedings of the Institution of Mechanical Engineers, Part E: Journal of Process Mechanical Engineering,* ***230***(3), pp. 183–197.

[39] Symétrie. Synchrotron Diffractometer. `http://www.symetrie.fr/en/applications-2/synchrotron-diffractometer/`. [Accessed: 2018-03-08].